Femtosecond laser activation of the photochemistry of Bismuth and associated threedimensional sub-micron fluorescence patterning

Fouad Alassani, Nadège Ollier, Lionel Canioni, Yannick Petit, Thierry Cardinal

Femtosecond laser activation of the photochemistry of Bismuth and associated three-dimensional sub-micron fluorescence patterning

Fouad Alassani[1,2], Nadège Ollier[2], Lionel Canioni[1], Yannick Petit[1], Thierry Cardinal[1]

[1] *Université de Bordeaux, CNRS, Bordeaux INP, ICMCB, UMR 5026, F-33600 Pessac, France*
[2] *Laboratoire des Solides Irradiés, UMR 7642 CEA-CNRS-Ecole Polytechnique, Palaiseau, France*

Abstract

Sub-micrometer 3D structures in a Bismuth-doped phosphate glass were achieved thanks to femtosecond direct laser writing. These structures exhibit high fluorescence contrast with good spatial resolution with spectral emission in the red and near-IR. These fluorescence properties arise from femtosecond laser-induced multi-photon absorption and the creation of free electrons, which activate local redox reactions of Bi^{3+} that allow for the formation of low valence bismuth ions such as Bi^{2+} and Bi^{+}. These new species promote not only new selective fluorescence emission properties in the VIS and near-IR spectral range but also co-localized positive refractive index changes. The thermal treatment of 3D patterns evidences the possibility of bismuth cluster formation with good thermal stability up to the glass temperature transition.

Keywords: Femtosecond Direct Laser Writing, Bimuth redox, Photoredox, Photochemistry, 3D patterning

1. Introduction

Bismuth-doped glasses have gained significant interest since the discovery of bismuth-related near-IR emission [1]. Near-IR emission of bismuth has been reported to be able to be excited across various domains of the visible spectrum (VIS), as well as to emit a long-lasting sub-millisecond-range broadband spectrum that encompasses the second telecommunication windows (O, E, S) [2]–[6]. This near-IR bismuth emission can have potential applications for laser amplification and tunable laser components. However, the origin of this near-IR emission has been subject to debate for many years, as it may result from the presence of several bismuth species while the dominant near-IR emitters are most likely Bi^{+} ions [7], [8]. The clustering of bismuth ions as a possible source of the near-IR emission has also been reported [9]. Additionally, alongside the near-IR emission, a red emission attributed to Bi^{2+} has also been documented [9]–[14]. These low valence bismuth ions (Bi^{+} and Bi^{2+}) are believed to result from the reduction of the most stable Bi^{3+} ions, for which the luminescence properties are located in

UV and VIS ranges [8], [9], [15], [16]. The unique ability of bismuth to exist in different oxidation states, each with distinct luminescence properties, makes it appear as a wonderful element [17]. Nevertheless, achieving precise control over the valence state of bismuth ions for specific applications remains a challenge, requiring careful selection of synthesis methods and glass hosts.

Generally, the introduction of low valence bismuth ions such as Bi^{2+} and Bi^{+} ions in glass can be achieved by the conventional glass synthesis technique in a reductive atmosphere [18], by heat treatment of the glass in a controlled atmosphere [18], [19], or by co-doping bismuth with other elements such as silver [18], [20]. These techniques facilitate the homogeneous distribution of the low-valence bismuth ions in the bulk glass. However, alternative methods such as femtosecond direct laser writing (fs DLW) for instance, offer powerful tools to tune local luminescence properties through local modification of the glass or space-selective permanent reduction of active metal ions [21]–[24]. A submicron-scale local material modification is achieved thanks to tightly focused femtosecond laser illumination and resulting nonlinear multiphoton absorption processes that lead to the formation of a plasma with a high density of free electrons at the interaction voxel. In the case of bismuth-doped glasses, such a cloud of free electrons can trigger local photo-reduction reactions of Bi^{3+}, leading to the formation of low valence bismuth ions with emitting luminescence properties in the red and near-IR range [25]–[30]. This capability opens the path to induce photonic functionalities and 3D architectures at the diffraction limit by locally tuning both fluorescence and refractive properties similarly to what has been broadly reported for silver-containing glasses [31], [32].

In this paper, we report on the fs DLW-induced 3D patterning of a bismuth-doped phosphate glass, which gives access to sub-micrometer 3D architectures with tunable local luminescence spanning from the red to the near IR ranges.

2. Experimental section

2.1 Synthesis of glass

We synthesized a zinc-phosphate glass (PZn) with the specific composition $38.5ZnO\text{-}56PO_{5/2}\text{-}5.5GaO_{3/2}$. The raw materials were subjected to a melting process at 1200°C for 2 hours. For the incorporation of bismuth, we ground 10 g of the synthesized PZn glass with 200 mg of Bi_2O_3 (Sigma-Aldrich, 99.9%) representing 2% of the mass of PZn glass. This resulted in an overall cationic composition of the bismuth-doped glass that writes $38.25ZnO\text{-}55.63PO_{5/2}\text{-}5.46GaO_{3/2}\text{-}0.65BiO_{3/2}$. The mixture underwent a melting process at 1200 °C for four hours

with intermediate grinding to ensure the homogenous distribution of bismuth ions in the glass. Following the melting process, the transparent glass was free from any discernible coloration and it was further annealed at 40 °C below its glass transition temperature (T_g = 430 °C) for four hours. Subsequently, the glass was cut into small 1 mm thick samples for optical polishing.

2.2 Femtosecond direct laser writing

3D fluorescent structures were induced by a Ytterbium femtosecond (fs) oscillator (up to 2.6 W, 9.1 MHz, and 390 fs FWHM at 1030 nm), combined with an acousto-optic modulator, that allows tuning pulse energies and associated irradiances up to 100 nJ and 20 $TW.cm^{-2}$, respectively. High-precision XMS-50 translation stages (up to 50 nm) allowed to move samples in 3D (40 nm repositioning resolution) during DLW irradiation. The laser beam was focused at 160 µm below the sample surface with a Zeiss microscope objective (40×, 0.75NA). A spatial light modulator (LCOS; X10468-03, Hamamatsu Photonics) was also used to correct spherical aberrations.

2.3 Confocal fluorescence imaging, refractive index change, micro luminescence spectroscopy

Confocal fluorescence imaging was performed using a Leica DM6 CFS TCS SP8 confocal microscope equipped with a 532 nm laser diode, and an immersion microscope objective (Leica, 63×, 1.3NA, index matching oil at n = 1.512). Images were recorded over the spectral range of 650-750 nm. Refractive index changes with respect to the pristine glass were analyzed with a phase-contrast microscopy method, equipped with the commercially available wave-front sensor SID4Bio from PHASICS. White light and a 100× – 1.3 NA oil immersion objective were used to image the structure.

Micro-luminescence spectroscopy was performed with a high spectral resolution micro-spectrometer (LabRAM HR800 from (Horiba Jobin Yvon GmbH, Germany) with 300 $grooves.cm^{-1}$ grating, using a Peltier-cooled CCD camera and a liquid nitrogen-cooled InGaAs detector to record the fluorescence spectra of the laser-inscribed structures. The 532 nm excitation source was a TEM_{00}, single-mode laser diode of 100 mW (Coherent, USA). An Olympus microscope objective (50×, 0.9 NA) was used for excitation and epi-collection.

For the electronic irradiation, the glass was continuously irradiated at LSI (Laboratoire des Solides Irradiés), Palaiseau, France, and supported by the French Network EMIR using the SIRIUS electron accelerator. 2.5 MeV electron beam is used in order to homogenously irradiate

0.7 mm thick glass samples, which sample holder was kept at room temperature with a water cooling system.

3. Results and Discussion

3.1 DLW-induced structural pattern

With the bismuth-doped glass (PZnBi), fs DLW has been performed to evaluate its photosensitivity. Snake-like patterns of 50×50 μm^2 size with an internal distance of 5 µm were created (Fig. 1) with a laser irradiance of 5.74 $TW.cm^{-2}$ and sample displacement velocity of 10 $\mu m.s^{-1}$. Under a 532 nm excitation source, this pattern shows a background-free high fluorescence contrast, as shown in Fig. 1a, demonstrating the capability of sub-micron similarly patterning the PZnBi glass to what has already been largely reported for silver-containing glasses [31], [32]. This fluorescence contrast recorded in the red spectral range is likely to be associated with the laser-created new species of bismuth ions, especially the Bi^{2+} ions that were not present before the laser inscription. Indeed during fs illumination, a high density of free electrons is generated, which can imply photo-redox reactions of bismuth elements. Additionally, the pattern exhibits double-track modifications that globally form at the edge of the voxel of laser/matter interaction resulting from the pulse-to-pulse photo-ionization and photo-dissociation of fluorescence species, similar to what was reported elsewhere for the case of silver clusters [32], [33]. Phase contrast imaging has also been performed (as shown in Fig. 1b), revealing the resulting laser-induced optical path difference. It shows a high phase contrast between the laser-modified area and the laser-free areas. The darker regions of the image match well with the laser-modified area, highlighting the double-track modification being perfectly co-localized with the fluorescence image. This phase contrast image allows for estimating a positive refractive index change of the double-track which is in the order of 10^{-3}. Indeed, this positive refractive index change may originate from the change of local electron density (implying laser-induced species migration and accumulation at the edge of the interaction voxel) and/or from the change of the polarizability of bismuth ions (implying the creation of new low valence bismuth ions). One may also suggest the formation of new molecular bonds between closely bismuth ions for which the polarization may contribute to the positive index change. As displayed in Fig. 1c, it is remarkable to observe that 1D normalized cross-sections of laser-induced fluorescence emission (from Fig. 1a) and refractive index modifications (from

Fig. 1b) appear as strictly co-localized. This allows us to conclude that both fluorescence properties and refractive index changes originate from the fs laser-created bismuth species.

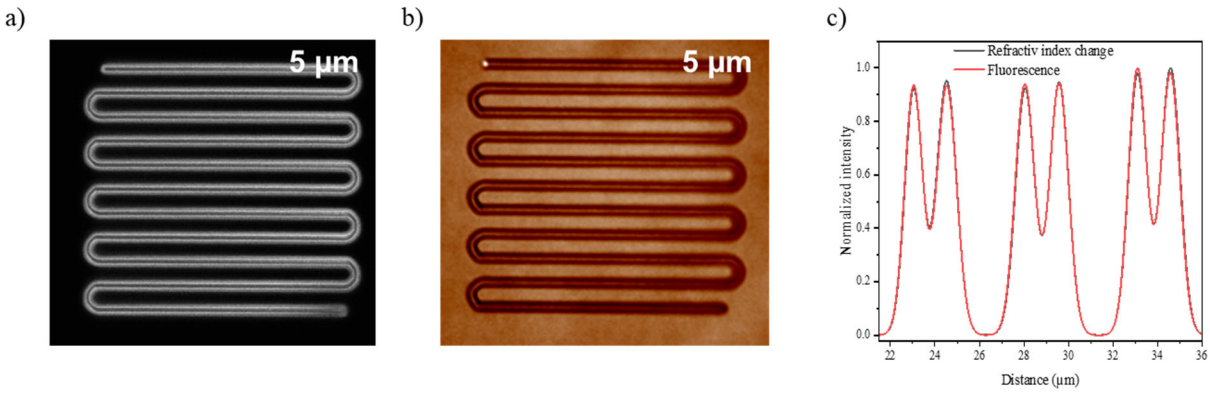

Fig 1. (a,b) High spatial resolution imaging of both (a) fluorescence and (b) phase contrast of a laser-inscribed structure (irradiation at 5.74 TW.cm^{-2} and 10 µm.s^{-1} with a pitch of 5 µm. (c) Superposition of normalized fluorescence and refractive index change profiles of three successive laser passes for the photo-inscribed structure from (a) and (b), respectively.

Furthermore, the behavior of laser-inscribed patterns has been investigated under laser pass overlapping and re-inscription approaches. This aspect deals with the possibility of erasing a pre-inscribed fluorescence track thanks to a successive laser pass by photo-cancelling pre-inscribed low valence Bismuth ions or potential Bismuth clusters, correlatively to the inscription of new Bismuth-sustained modification tracks. Such an approach shall offer the ability to create patterns with adjustable periodicities, such periodicities being not limited by the laser/matter interaction voxel, but only by the sub-micron inner thickness on an individual track, similar to what is reported in silver-containing glasses [32], [33]. In the present case of PZnBi glass, as shown in Fig. 2a, we have inscribed first a vertical double-track and subsequently a second horizontal double-track in the same plane, but perpendicularly and intersecting the first double-track in the middle. The result reveals that the second laser pass can erase the initial fluorescence double-track at the intersection point, leaving in the areas framed in red, residual tracks that show much weaker fluorescence emission. This highlights the occurrence of a photo-dissociation reaction of the pre-inscribed fluorescence species as well as the photo-creation of new fluorescent tracks with lower writing efficiency in the area where a first laser pass had already taken place. While considering now parallel laser overlapping with separation distances (between successive laser passes) smaller than the typical voxel lateral size, it allows for inscribing patterns with internal periodicity ranging from 1 µm to 0.25 µm, as shown in Figs. 2b and 2c, respectively. For the 1 µm interspacing pattern, which closely matches the size of the laser spot, the successive laser passes overlap once, resulting in a well-contrasted periodic pattern with a 1 µm pitch. In contrast, when the inter-distance is reduced to

about 0.25 µm, the resulting pattern tends to appear as a densely packed matrix since the resolution of our apparatus is insufficient to distinguish individual features within such a dense matrix.

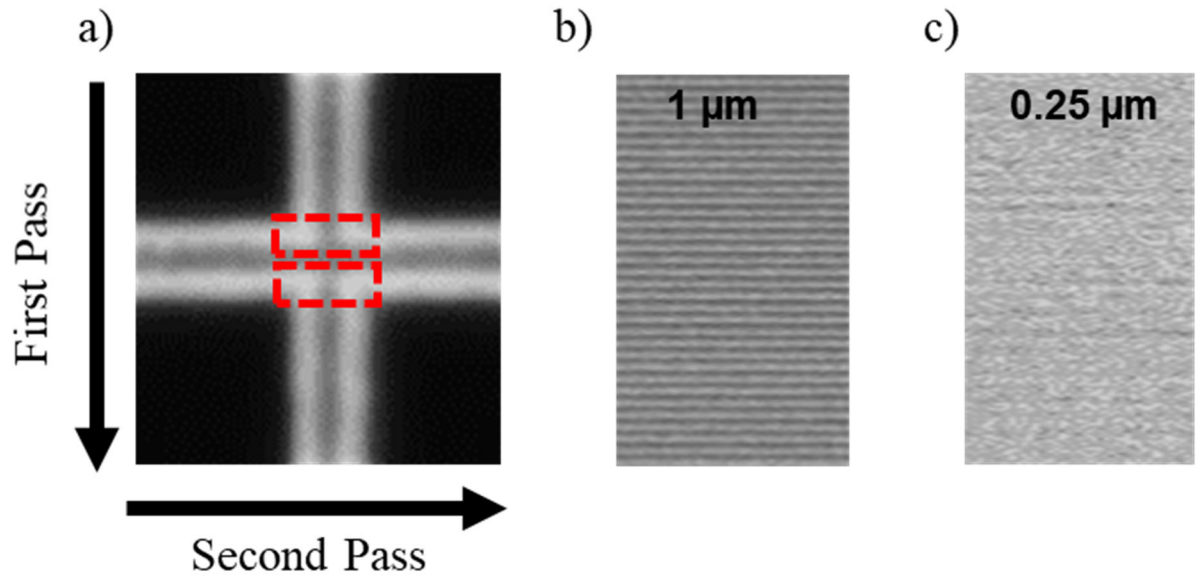

Fig 2. Confocal fluorescence images: (a) crosswriting of the photo-induced structure evidencing the photo-dissociation process of the first double track; (b,c) laser-inscribed structure with a pitch of 1 µm and 0.25 µm, respectively.

3.2 Confocal micro-emission spectroscopy

To determine the origin of the fluorescence properties of the DLW-induced patterns, the confocal micro emission spectroscopy has been performed with a series of laser-created patterns obtained at various laser irradiances from 3.7 TW.cm^{-2} to 5.74 TW.cm^{-2} and fixed sample velocity of 10 µm.s^{-1}. Figure 3a displays the confocal fluorescence image of these patterns under excitation at 532 nm. This evidences an increase in the fluorescence intensity with the increase of the laser irradiance. Furthermore, the emission spectrum of the pattern is inscribed with 3.70 TW.cm^{-2} (Fig. 3b) reveals a broad emission band covering the whole red region, *i.e.* starting from 600 nm to 800 nm with the main maximum at 720 nm and an additional shoulder around 680 nm. This emission has been associated with the $^2P_{3/2} \rightarrow {}^2P_{1/2}$ transition of Bi^{2+} ions [9]–[14], confirming the creation of Bi^{2+} ions in the laser-irradiated area. The additional shoulder can also be associated with Bi^{2+} ions located in a different environment. When recording the emission spectra in the near-IR range, we observe a broad emission band starting from 900 nm up to 1400 nm with a maximum at 1126 nm, as shown in Fig. 3c, which is attributed to the reported $^3P_1 \rightarrow {}^3P_0$ transition of Bi^{+} ions [8], [15], [19]. The intensity of both emission bands of each of the laser-created bismuth ions (Bi^{2+} and Bi^{+}) increases with increasing laser

irradiance (see Fig. 3b and Fig. 3b, respectively). Indeed, higher laser irradiances promote higher concentrations of free electrons, and subsequently larger amounts of phot-reductive reactions that favor the formation of these two new low-valence Bismuth ions. Note that both the red and near-IR emissions were collected from the same laser-irradiated areas, indicating the typical co-location of the red emitter Bi^{2+} and of the near-IR emitter Bi^{+}.

Indeed, the interaction of the fs laser with PZnBi glass leads to multiphoton absorption and photo-ionization at the root of out-of-equilibrium processes in the glass matrix. During these processes, a high density of laser-created free electrons and holes can then participate in the photo-reduction of Bi^{3+}, leading to the formation of low valence Bi^{2+} and Bi^{+} ions. Consequently, it becomes possible to achieve highly spatially selective modifications in the PZnBi glass, enabling the creation of sub-micrometer 3D structures, exhibiting remarkably broadband fluorescence properties that result from the concomitant formation of two distinct new Bismuth ion species with increasing fluorescence magnitude as the laser irradiance increases (Fig. 3b and Fig 3b). The photo-reduction reaction governing the formation of these low-valence bismuth ions can be expressed as follows:

$$\text{PZnBi glass} + h\nu \rightarrow e^{-} + h^{+}$$

$$Bi^{3+} + e^{-} \rightarrow Bi^{2+}$$

$$Bi^{2+} + e^{-} \rightarrow Bi^{+}.$$

Similarly to silver-containing glasses, the occurrence of double-track modifications produced after a laser pass (as shown in Fig. 1) demonstrates that the overall laser/matter interaction leads successively to the pulse-after-pulse budget that combines photo-redox creation of new species and their photo-dissociation. During laser irradiance, a given laser pulse promotes the reduction of Bi^{3+} to create Bi^{2+} species, while pre-existing Bi^{2+} species can get either oxidized to restore the Bi^{3+} population or further reduced in Bi^{+}. One might thus expect the pulse-to-pulse destruction of Bi^{2+} ions in the region of high laser energy in the center of the voxel of interaction, leading to a higher concentration of Bi^{2+} ions in the region of low laser energy at the periphery of the laser spot. Indeed, the double track arises from the linear translation of the glass sample in a direction perpendicular to the laser propagation, allowing the destruction of Bi^{2+} by the front side of the laser voxel without their recreation at its backside. Based on Figs. 1-3, the resulting spatial distribution of new Bismuth species appears quite similar to that achieved in 3D nanostructures of silver clusters in silver-containing glasses [32]–[34].

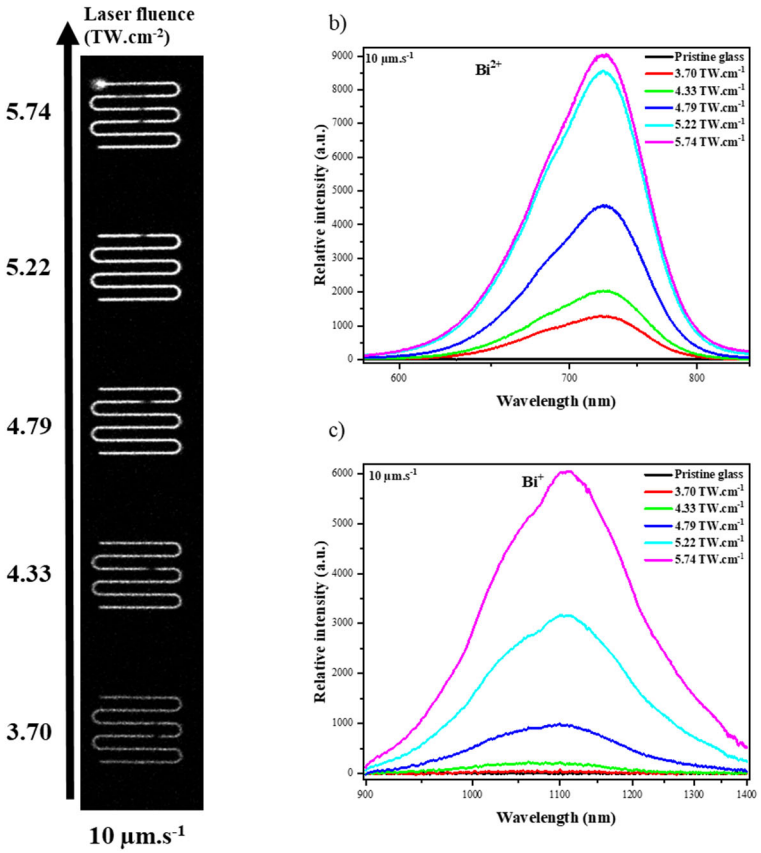

Fig 3. (a) Confocal fluorescence image for 532 nm excitation of DLW-induced structures with various laser irradiances from 3.70 TW.cm^{-2} to 5.74 TW.cm^{-2} and at fixed sample velocity of 10 µm.s^{-1}. (b,c) Confocal micro-emission spectra of the DLW-induced structure under 532 nm excitation illustrate for different irradiances the emission spectra of Bi^{2+} and Bi^{+}, respectively.

3.3 Thermal stability of the laser-created fluorescent centers

The influence of the heat treatment on the fluorescence response of the fs laser-induced patterns has been performed to evaluate the thermal stability of the luminescence centers. The pattern inscribed with 5.74 TW.cm^{-2} and 10 µm.s^{-1} was submitted to heat treatment from room temperature to 430 °C (T_g) with steps of 40 °C. The sample was held for 30 minutes at each temperature, and then cooled to room temperature for micro-luminescence analysis. Figure 4a displays the spectral integration of the Bi^{2+} emission when temperature is increasing. The spectral integration starts to increase with temperature: it reaches its maximum intensity at 175°C and then decreases when the temperature increases up to T_g. The initial increase of the spectral integration corresponds to the initial creation and augmentation of Bi^{2+} ions, facilitated by the recombination of relaxed electrons with the remaining Bi^{3+} ions. Conversely, the

subsequent decrease of the spectral integration may stem from ongoing temperature-influenced redox reactions, where Bi^{2+} ions can be oxidized to Bi^{3+} or reduced to Bi^{+}, as globally depicted in the following equation:

$$2Bi^{2+} + e^{-} + h^{+} \rightarrow Bi^{3+} + Bi^{+}$$

The normalization of the Bi^{2+} spectra at different temperatures, as depicted in Fig. 4c, reveals that there is no significant change in the spectra so their environment is not significantly affected. Only slight shifts, attributed to the temperature-induced local rearrangement of Bi^{2+} ions are observed. In the case of Bi^{+} ions, the spectral integration of the near-IR spectrum follows a similar thermal dependence, as shown in Fig. 4b. However, the maximal emission is reached at 225°C, at the temperature where Bi^{2+} spectral integration has already started to drop (as seen in Fig. 4a). This feature corroborates the dependence of the Bi^{+} ions with respect to the Bi^{2+} ions that undergo a second reduction step, showcasing the transition of Bi^{2+} to Bi^{+} at higher temperature. At this stage, Bi^{+} is considered as the final product all along the redox process of Bi^{3+}. Above 300 °C, both Bi^{2+} and Bi^{+} ions show lower thermal stability with strongly reduced emission intensity, suggesting their full oxidation and the restoration of the Bi^{3+} population.

The normalized spectra of Bi^{+} ions depicted in Fig. 4d reveal significant spectral changes when temperature increases since a new contribution appears between 1200 and 1350 nm at 175 °C. The associated near-IR intensity relatively increases when the temperature increases up to 305°C. Subsequently, at 350 °C, a strong shift to lower wavelengths is observed, which is associated with the decrease of the latter contribution and the main contribution at 1126 nm. Meanwhile, a new contribution appears around 1076 nm. These features are attributed to the existence of another type of emitting centers such as bismuth cluster families. Some types of Bismuth clusters are created during DLW and further experience good thermal stability. while other types are favored by thermal treatment [3], [35]. Indeed, laser inscription can induce an out-of-equilibrium process so that bismuth ions can agglomerate and start to form close-packed molecular clusters with initially deficient or in-excess electron charges [25]. Moreover, the substantial reduction in the emission intensity of Bi^{2+} and Bi^{+} can be attributed to thermally activated reactions involving the consumption of these two ions to the formation of non-luminescent metallic bismuth or bismuth clusters [36].

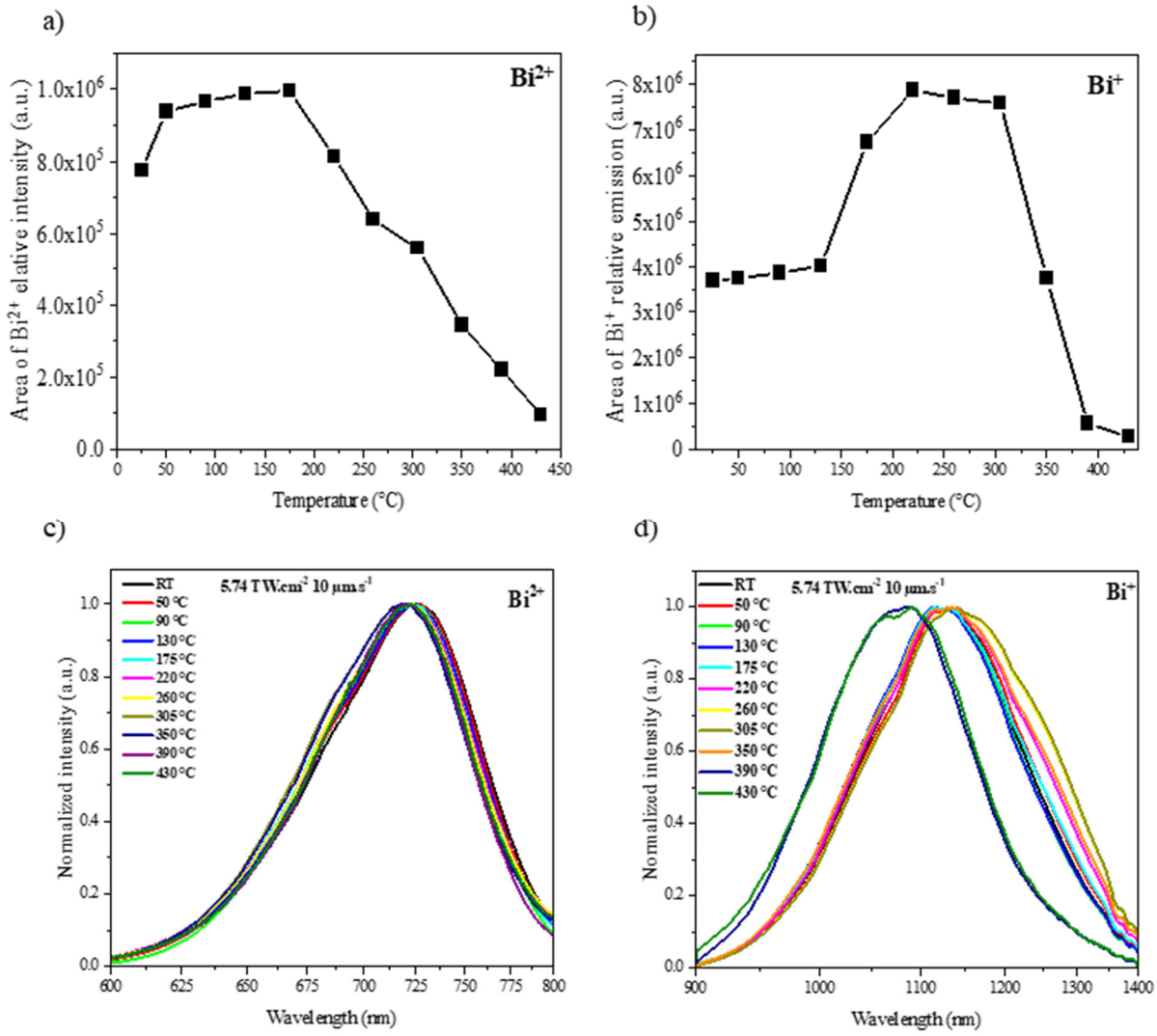

Fig 4. (a,b) Trend of spectral integration of Bi^{2+} and Bi^{+} respectively at different temperatures;(c,d) normalized thermal dependent of the emission spectra of Bi^{2+} and Bi^{+} species, respectively.

3.4 Electron irradiation versus femtosecond irradiation

As demonstrated here above, laser inscription enables to promote local modifications with sub-diffraction features in the present PZnBi glass, in a quite similar manner to what is largely reported in silver-containing glasses. Such a modification is achieved thanks to photo-redox reactions supported by Bismuth ions. As the volume of the laser/matter interaction voxel is very small (a few μm^3) and because the laser-induced free electrons lead to an initial highly out-of-equilibrium state, it is not straightforward to access the initial phenomenon of glass modification. Hence, a 2.5 MeV electron irradiation has been performed to access a larger volume of interaction suitable for macro-spectroscopy, as well as much lower free electron densities. Figure 5a displays the linear absorption spectroscopy of the electron-irradiated glass

and the pristine glass. The result reveals the creation of multiple absorption bands after electron irradiation, which encompasses the visible range with the main contribution around 500 nm, a smaller band in the red range with a peak maximum of around 696 nm, and a shoulder around 804 nm. This indicates the presence of different photoactive species such as Bi^{2+} and Bi^{+} after electronic irradiation. Additionally, the electron-irradiated glass becomes more absorbent in the UV range with a strong red shift of the absorption tail. An additional absorption band between 350 nm and 400 nm may correspond to point defects formed in the phosphate matrix whose specific origin is not identified at this stage. To ensure the presence of these ions, photoluminescence spectroscopy of the electron-irradiated glass was performed. Figure 5b displays the emission spectrum for a 550 nm excitation and the excitation spectrum monitored for a 720 nm emission. For the 550 nm excitation, the characteristic red emission band of Bi^{2+} (with maximum 720 nm) emerges and shares similarity with that observed for the fs DLW patterns in Fig. 3b. While the excitation spectrum monitored for the 720 nm emission reveals a broad excitation band covering the entire visible range (400-700 nm) with a maximum at 580 nm associated with the Bi^{2+} absorption. For the near-IR luminescence spectroscopy shown in Fig. 5c, we also observe the characteristic emission band of Bi^{+}, also sharing similarities to what was observed in the fs DLW patterns (Fig. 3c) [4]. The corresponding excitation band of this near-IR emission, monitored for an emission at 1100 nm exhibits a broad excitation band covering the entire visible range (370-800 nm), with two main contributions centered at 515 nm and 696 nm, respectively. These excitation bands (attributed to Bi^{+} ions) are in agreement with what is observed elsewhere in other Bi-doped glass [4]. Additional sharp peaks marked with stars at 656 and 830 nm are also observed: their origin is unknown yet. It is noticeable that the excitation band at 696 nm for the emission at 1100 nm corresponds well to the contribution at 696 nm in the linear absorption spectrum of the electron-irradiated glass, which supports the presence of Bi^{+} ions. However, the broad contribution around 500 nm in the linear absorption spectrum may be described as a linear combination of excitation bands of Bi^{2+} ions and Bi^{+} ions, as suggested by excitation spectra from Fig. 5b and 5c. The additional shoulder around 808 nm has been reported to be associated with Bi^{+} ions [37].

Furthermore, time-resolved spectroscopy was performed for a 355 nm excitation with emission collected at 720 nm, as shown in Fig. 5c, exhibiting an exponential decay curve fitted with tree-independent exponential components. The shortest lifetime of 43 ns should not be considered as it is likely to be due to the experimental artifacts. The longer lifetime of 3.17 µs is likely to be associated with Bi^{2+} [38]. The 0.79 µs lifetime may either be associated with Bi^{2+} ions too

but in different environments, or it may result from energy transfer mechanisms that tend to reduce the associated lifetime. The time-resolved spectroscopy in the near-IR emission could not be investigated here for experimental reasons.

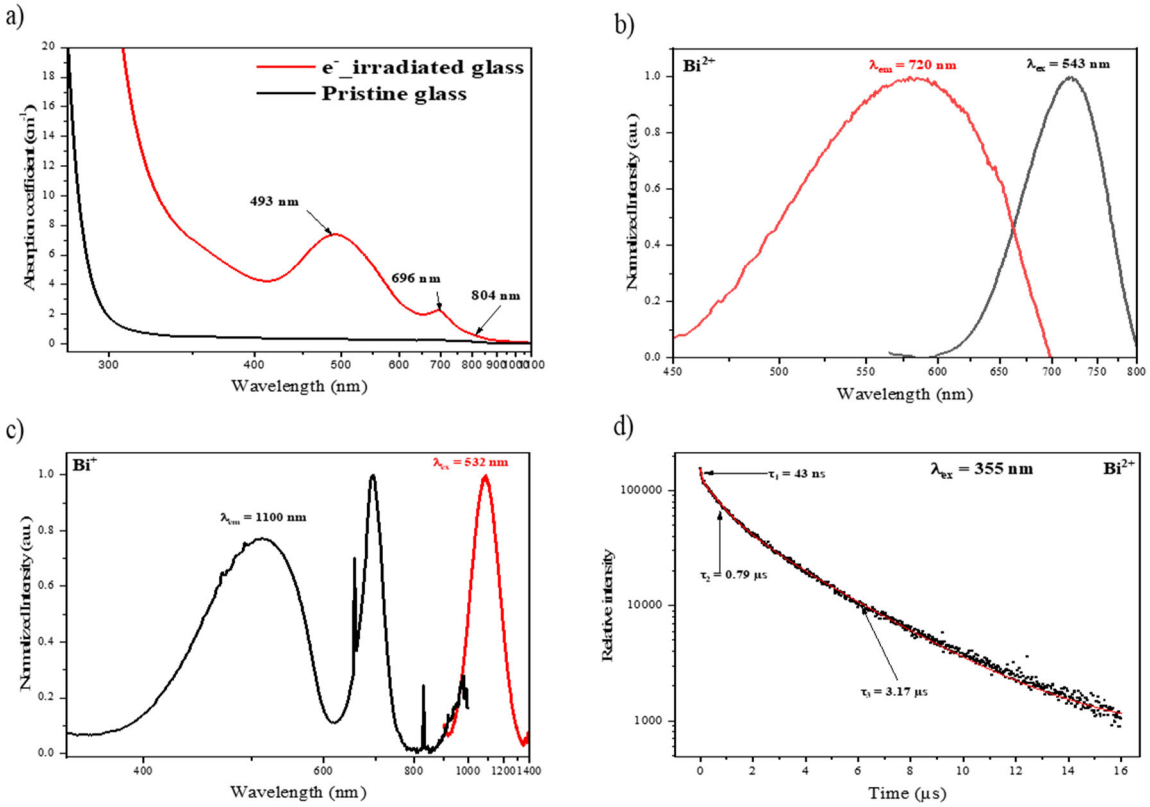

Fig 5. (a) Absorption spectroscopy of a PZnBi glass irradiated with a 2.5 MeV electron beam; (b,c) excitation and emission spectra of electron-irradiated PZnBi glass for Bi^{2+} and Bi^{+}, respectively; (d) time-resolved spectroscopy of Bi^{2+} for excitation at 550 nm and collection at 720 nm.

4. Conclusion

The present investigation has demonstrated the unique capability to engineer 3D fluorescent and refractive structures within a bismuth-containing PZn glass, while locally playing on the oxidation state of bismuth species thanks to tightly focused femtosecond laser irradiation. First, the introduction of Bi^{3+} with good stability has been achieved in a phosphate glass. Luminescence spectroscopy has allowed evidencing that the valence reduction of Bi^{3+} to low valence bismuth ions Bi^{2+} and Bi^{+} occurs under ionizing irradiation such as femtosecond laser or electron beam irradiations. Femtosecond laser inscription promotes such photo-redox reactivity and allows for the creation of 3D structures that exhibit co-localized background-free fluorescence contrast and refractive index change, both modifications arising from the formation of Bi^{2+} and Bi^{+} ions. The co-localization of the Bi^{2+} fluorescence emission and the

refractive index change have been observed. A strong correlation between fs DLW and electronic irradiation has been evidenced, showing that the low valence bismuth ions created by the two techniques are similar. Thanks to the electron irradiation, the absorption and luminescence spectroscopy of Bi^{2+} and Bi^{+} ions is well resolved. Femtosecond laser-induced 3D structures exhibit sub-micron spatial resolutions with species-selective fluorescence emission in the red and near-IR range, making them promising candidates for applications in bio-imaging systems, micro-tunable lasers, and photonic integrated circuits in the near-IR domains.

Acknowledge: This research has benefited from financial support from the French National Research Agency (ANR) ANR-19-CE08-0021-01 and Région Nouvelle Aquitaine (project AAPR2020-2019-8193110). We acknowledge the financial support from the Grand Research Program « LIGHT » Idex University of Bordeaux, and the Graduate program « EUR Light S&T » PIA3 ANR-17-EURE-0027. Electron beam irradiation experiments were performed at LSI (Laboratoire des Solides Irradiés), Palaiseau, France, and supported by the French Network EMIR.

References

[1] Y. Fujimoto and M. Nakatsuka, “Infrared luminescence from bismuth-doped silica glass,” *Japanese J. Appl. Physics, Part 2 Lett.*, vol. 40, no. 3 B, Mar. 2001, doi: 10.1143/JJAP.40.L279.

[2] X. Meng *et al.*, “Near infrared broadband emission of bismuth-doped aluminophosphate glass,” *Opt. Express*, vol. 13, no. 5, p. 1628, 2005, doi: 10.1364/OPEX.13.001628.

[3] M. Peng, J. Qiu, D. Chen, X. Meng, and C. Zhu, “Superbroadband 1310 nm emission from bismuth and tantalum codoped germanium oxide glasses,” *Opt. Lett.*, vol. 30, no. 18, p. 2433, Sep. 2005, doi: 10.1364/OL.30.002433.

[4] Z. J. Yong, Y. Zhou, B. M. Liu, D. D. Zhou, and H. T. Sun, “A Soft Chemistry-Based Route to Near-Infrared Luminescent Bismuth-Activated Glass Films,” *J. Am. Ceram. Soc.*, vol. 100, no. 1, pp. 133–140, 2017, doi: 10.1111/JACE.14563.

[5] Y. Fujimoto and M. Nakatsuka, “Optical amplification in bismuth-doped silica glass,” *Appl. Phys. Lett.*, vol. 82, no. 19, pp. 3325–3326, 2003, doi: 10.1063/1.1575492.

[6] J. Ni *et al.*, “Study on pump optimizing for Bi/Er co-doped optical fiber,” *Measurement*, vol. 79, pp. 160–163, Feb. 2016, doi: 10.1016/J.MEASUREMENT.2015.10.003.

[7] X. Meng *et al.*, “Infrared broadband emission of bismuth-doped barium-aluminum-borate glasses,” *Opt. Express*, vol. 13, no. 5, p. 1635, 2005, doi: 10.1364/OPEX.13.001635.

[8] J. Ren, J. Qiu, D. Chen, X. Hu, X. Jiang, and C. Zhu, “Luminescence properties of bismuth-doped lime silicate glasses,” *J. Alloys Compd.*, vol. 463, no. 1–2, pp. L5–L8, Sep. 2008, doi: 10.1016/J.JALLCOM.2007.09.026.

[9] B. I. Denker, B. I. Galagan, I. L. Shulman, S. E. Sverchkov, and E. M. Dianov, “Bismuth valence states and emission centers in Mg-Al-silicate glass,” *Appl. Phys. B Lasers Opt.*, vol. 103, no. 3, pp. 681–685, Jun. 2011, doi: 10.1007/S00340-010-4241-1.

[10] J. Ren, J. Qiu, D. Chen, X. Hu, X. Jiang, and C. Zhu, “Luminescence properties of bismuth-doped lime silicate glasses,” *J. Alloys Compd.*, vol. 463, no. 1–2, Sep. 2008, doi: 10.1016/J.JALLCOM.2007.09.026.

[11] M. Peng and L. Wondraczek, “Bi^{2+}-doped strontium borates for white-light-emitting diodes,” *Opt. Lett.*, vol. 34, no. 19, p. 2885, Oct. 2009, doi: 10.1364/OL.34.002885.

[12] H. K. Dan, A. L. Phan, N. M. Ty, D. Zhou, and J. Qiu, “Optical bandgaps and visible/near-infrared emissions of Bi^{n+}-doped (n = 1, 2, and 3) fluoroaluminosilicate glasses via Ag^{+}-K^{+} ions exchange process,” *Opt. Mater. (Amst).*, vol. 112, p. 110762, Feb. 2021, doi: 10.1016/J.OPTMAT.2020.110762.

[13] P. Dang, D. Liu, G. Li, A. A. Al Kheraif, and J. Lin, “Recent Advances in Bismuth Ion-Doped Phosphor Materials: Structure Design, Tunable Photoluminescence Properties, and Application in White LEDs,” *Adv. Opt. Mater.*, vol. 8, no. 16, 2020, doi: 10.1002/adom.201901993.

[14] A. M. Srivastava, “Luminescence of divalent bismuth in M^{2+} BPO5 (M^{2+} = Ba^{2+}, Sr^{2+} and Ca^{2+}),” *J. Lumin.*, vol. 78, no. 4, pp. 239–243, Jun. 1998, doi: 10.1016/S0022-2313(98)00010-6.

[15] G. Chi, D. Zhou, Z. Song, and J. Qiu, “Effect of optical basicity on broadband infrared fluorescence in bismuth-doped alkali metal germanate glasses,” *Opt. Mater. (Amst).*, vol. 31, no. 6, pp. 945–948, 2009.

[16] B. Niu, L. Zhao, S. Liu, H. Dong, and H. Yu, “Single band luminescence of Bi^{3+} and the intensity modulation in potassium borosilicate glasses,” *J. Non. Cryst. Solids*, vol. 581, no. November

2021, p. 121421, 2022, doi: 10.1016/j.jnoncrysol.2022.121421.

[17] H. K. Dan, A. L. Phan, N. M. Ty, D. Zhou, and J. Qiu, "Optical bandgaps and visible/near-infrared emissions of Bi^{n+}-doped (n = 1, 2, and 3) fluoroaluminosilicate glasses via Ag^{+}-K^{+} ions exchange process," *Opt. Mater. (Amst).*, vol. 112, Feb. 2021, doi: 10.1016/J.OPTMAT.2020.110762.

[18] Y. Arai, T. Suzuki, Y. Ohishi, S. Morimoto, and S. Khonthon, "Ultrabroadband near-infrared emission from a colorless bismuth-doped glass," *Appl. Phys. Lett.*, vol. 90, no. 26, 2007, doi: 10.1063/1.2752539.

[19] A. You, M. A. Y. Be, and I. In, "Study of thermal stability and luminescence quenching properties of bismuth-doped silicate glasses for fiber laser applications," vol. 041908, no. December 2007, pp. 90–93, 2008, doi: 10.1063/1.2828035.

[20] X. He, X. Xu, Y. Shi, and J. Qiu, "Effective enhancement of Bi near-infrared luminescence in silicogermanate glasses via silver-sodium ion exchange," *J. Non. Cryst. Solids*, vol. 409, pp. 178–182, 2015, doi: 10.1016/j.jnoncrysol.2014.11.021.

[21] J. Qiu *et al.*, "Space-selective valence state manipulation of transition metal ions inside glasses by a femtosecond laser," *Appl. Phys. Lett.*, vol. 79, no. 22, pp. 3567–3569, Nov. 2001, doi: 10.1063/1.1421640.

[22] J. Qiu, K. Kojima, K. Miura, T. Mitsuyu, and K. Hirao, "Infrared femtosecond laser pulse induced permanent reduction of Eu^{3+} to Eu^{2+} in a fluorozirconate glass," *Opt. Lett.*, vol. 24, no. 11, p. 786, Jun. 1999, doi: 10.1364/OL.24.000786.

[23] K. Miura, J. Qiu, S. Fujiwara, S. Sakaguchi, and K. Hirao, "Three-dimensional optical memory with rewriteable and ultrahigh density using the valence-state change of samarium ions," *Appl. Phys. Lett.*, vol. 80, no. 13, pp. 2263–2265, Apr. 2002, doi: 10.1063/1.1459769.

[24] J. Qiu, K. Miura, T. Suzuki, T. Mitsuyu, and K. Hirao, "Permanent photoreduction of Sm^{3+} to Sm2+ inside a sodium aluminoborate glass by an infrared femtosecond pulsed laser," *Appl. Phys. Lett.*, vol. 74, no. 1, pp. 10–12, Jan. 1999, doi: 10.1063/1.123117.

[25] V. Kononenko *et al.*, "Activation of color centers in bismuth glass by femtosecond laser radiation," *Laser Phys.*, vol. 21, no. 9, pp. 1585–1592, 2011, doi: 10.1134/s1054660x1116002x.

[26] W. Yang, C. Corbari, P. G. Kazansky, K. Sakaguchi, and I. C. Carvalho, "Low loss photonic components in high index bismuth borate glass by femtosecond laser direct writing," *Opt. Express*, vol. 16, no. 20, p. 16215, 2008, doi: 10.1364/oe.16.016215.

[27] L. Wang *et al.*, "In situ instant generation of an ultrabroadband near-infrared emission center in bismuth-doped borosilicate glasses via a femtosecond laser," *Photonics Res.*, vol. 7, no. 3, p. 300, 2019, doi: 10.1364/prj.7.000300.

[28] N. D. Psaila *et al.*, "Femtosecond laser inscription of optical waveguides in bismuth ion doped glass," *Opt. InfoBase Conf. Pap.*, vol. 14, no. 22, pp. 1515–1517, 2007, doi: 10.1364/oe.14.010452.

[29] M. Peng, Q. Zhao, J. Qiu, and L. Wondraczek, "Generation of Emission Centers for Broadband NIR Luminescence in Bismuthate Glass by Femtosecond Laser Irradiation," *J. Am. Ceram. Soc.*, vol. 92, no. 2, pp. 542–544, Feb. 2009, doi: 10.1111/j.1551-2916.2008.02909.x.

[30] S. Zhou, W. Lei, J. Chen, J. Hao, H. Zeng, and J. Qiu, "Laser-induced optical property changes inside Bi-doped glass," *IEEE Photonics Technol. Lett.*, vol. 21, no. 6, pp. 386–388, 2009, doi: 10.1109/LPT.2008.2011749.

[31] Y. Petit *et al.*, "On the femtosecond laser-induced photochemistry in silver-containing oxide glasses: Mechanisms, related optical and physico-chemical properties, and technological

applications," *Adv. Opt. Technol.*, vol. 7, no. 5, pp. 291–309, Oct. 2018, doi: 10.1515/AOT-2018-0037.

[32] T. Guérineau *et al.*, "Laser Direct Writing of Silver Clusters-Based Subwavelength Periodic Structures Embedded in Glass, Mid-infrared Gallo-germanate," vol. 2200032, 2022, doi: 10.1002/adpr.202200032.

[33] R. Laberdesque *et al.*, "Three-dimensional femtosecond laser inscription of type a-based high-efficiency first-order waveguide Bragg gratings," *Adv. Opt. Technol.*, vol. 12, p. 1237679, Jul. 2023, doi: 10.3389/AOT.2023.1237679.

[34] Y. Petit *et al.*, "Three-Dimensional High Spatial Localization of Efficient Resonant Energy Transfer from Laser-Assisted Precipitated Silver Clusters to Trivalent Europium Ions," *Cryst. 2021, Vol. 11, Page 148*, vol. 11, no. 2, p. 148, Feb. 2021, doi: 10.3390/CRYST11020148.

[35] M. Peng, D. Chen, J. Qiu, X. Jiang, and C. Zhu, "Bismuth-doped zinc aluminosilicate glasses and glass-ceramics with ultra-broadband infrared luminescence," *Opt. Mater. (Amst).*, vol. 29, no. 5, pp. 556–561, 2007.

[36] E. M. Dianov, "Bismuth-doped optical fibers: a challenging active medium for near-IR lasers and optical amplifiers," *Light Sci. Appl. 2012 15*, vol. 1, no. 5, pp. e12–e12, May 2012, doi: 10.1038/lsa.2012.12.

[37] J. Ren, J. Qiu, D. Chen, X. Hu, X. Jiang, and C. Zhu, "Luminescence properties of bismuth-doped lime silicate glasses," *J. Alloys Compd.*, vol. 463, no. 1–2, Sep. 2008.

[38] B. Denker, B. Galagan, V. Osiko, S. Sverchkov, E. Dianov, and A. M. Prokhorov, "Applied Physics B Luminescent properties of Bi-doped boro-alumino-phosphate glasses Basic properties of the BAP glass containing Al 2 O 3 6% and Bi 2 O 3 1%," *Appl. Phys. B*, vol. 87, pp. 135–137, 2007, doi: 10.1007/s00340-006-2518-1.